Journal of Physical Chemistry C 123.32 (2019): 19625-19636

DOI: https://doi.org/10.1021/acs.jpcc.9b04898

Outstanding Energy Exchange Between Organic Molecules and Metal Surfaces: Decomposition Kinetics Of Excited Vinyl Derivatives Driven By The Interaction With A Cu(111) Surface

Fernando Aguilar-Galindo[†] and Sergio Díaz-Tendero[*,†,‡,¶]

†*Departamento de Química - Módulo 13 - Universidad Autónoma de Madrid -28049 Madrid - Spain.*

‡*Condensed Matter Physics Center (IFIMAC), Universidad Autónoma de Madrid -28049 Madrid - Spain.*

¶*Institute for Advanced Research in Chemical Sciences (IAdChem), Universidad Autónoma de Madrid -28049 Madrid - Spain.*

E-mail: sergio.diaztendero@uam.es

Abstract

Here we present a thorough theoretical study of the interaction, chemisorption and thermal decomposition of three vynil derivatives (acrolein, acrylonitrile, and acrylamide) on a pristine Cu(111) surface. To this we have carried out density functional theory simulations, including weak van der Waals forces, in the framework of periodic boundary conditions. The results have shown strong anchoring between the molecules and the surface through the vinyl group, with the different functional groups driving

molecular orientation. We explain the chemisorption with a simple chemical picture: donation from the occupied lone pair and π orbitals of the molecule to the surface and backdonation from the surface to the π^* orbital of the molecule (π-backbonding). *Ab initio* molecular dynamics simulations highlight the efficient energy exchange in excited adsorbed molecules and energy dissipation through the interface, which takes place in a few hundreds of femtoseconds. The study of the dynamics also allows to comprehend the catalytic effect of the chemisorption, which is reflected not only in the larger amount of fragmentation but also in the much richer spectrum of fragments observed with respect to the molecular decomposition in gas phase.

Introduction

Interaction of organic molecules with metal surfaces has been studied for a long time (see e.g.[1–3]). Nevertheless it still remains as a hot topic due to the recent experimental developments that allow high precision in single molecule measurements and due to the number of applications in which it is involved.[4–6] In the case of transition metal substrates, the *d*-band of the surface is able to mix with some of the molecular states, in particular with the π states, since they are typically close in energy and spatially accessible, as stated in the *d-band center theory.*[7–11] These interactions can be explained with simple chemical models in terms of electron donation and back-donation[12] and are the responsible of the appearance of new properties in hybrid organic-metal materials, which are not present in the organic nor in the metal parts separately. For this reason, this kind of composite systems has been proposed as promising candidates in several areas such as hybrid metal-organic materials,[13–22] photovoltaic organic nanodevices,[23–26] ultrathin optoelectronics,[27–31] organic solar cells,[24,26,32,33] molecular spintronics,[34–37] corrosion protectors,[29,38–41] etc. In addition, the organic-metal interface is also responsible of a rearrangement of the molecular electron density that weakens some chemical bonds, while others become stronger, thus changing the intrinsic reactivity. This is the key aspect behind heterogeneous catalysis.[42–48] Other aspect that must be con-

sidered for catalytic applications is the anchoring of the molecule to the surface: as it has been recently pointed out by Jiang and Huo,[49] relative orientations of the adsorbed reactants and/or changes in the molecule-surface interaction energies enhance reaction rates; they further show the importance of the dynamics in these processes.

Excitation of vibrational modes is an excellent way to promote the system to higher energy states that are close to the so-called transition state (TS) point in the potential energy surface (PES), facilitating the reaction by increasing its rate. Nowadays it is possible to use light sources (typically ultrashort laser pulses) to selectively probe vibrational excited states that populate a given mode and thus, to drive the reaction through a specific path (the so-called quantum control[50–57]). For example, combination of different lasers allowed to probe the dynamics of all adsorbed molecules in a sample and selectively probe only different subsets of the adsorbed molecules in the same experiment.[58] Laser pulses have been also used to observe electronic structure changes in molecule-metal surface bond breaking employing a pump probe scheme;[59] the delay between the pump and the probe pulses allows measuring molecular desorbtion dynamics. Scanning tunneling microscopes (STM) have been also utilized in the promotion and control of single-molecule chemical reactions adsorbed on surfaces[60] through inelastic electron scattering processes: *cis-trans* isomerization,[61,62] molecular dissociation,[63] bond cleavage,[64,65] and dehydrogenation[66] are examples of single-molecule reactions induced with STM. The intermediate excited state created with the electric current of the STM is the key point to control these reactions. Recent experiments have studied in detail these electronic excited states in different systems.[67–69] Photo-assisted activation of selected bonds in individual molecules adsorbed on metal surfaces within the junction of a STM has been recently reported;[70] the mechanism behind this achievement consists in the coupling of photons with the bond activation through a resonant photo-assisted tunneling process.

Another important aspect that must be considered in the excitation of molecules that interact with metal surfaces is the energy relaxation mechanisms, i.e., the energy transfer

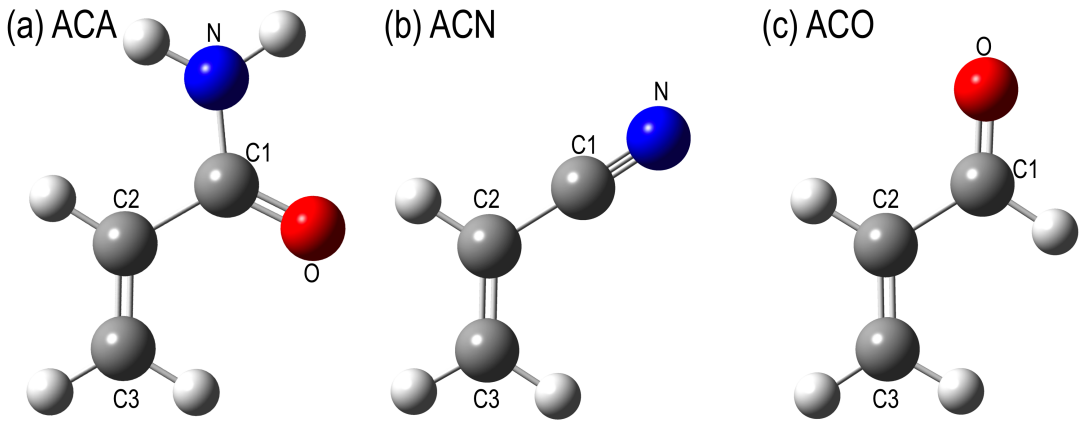

Figure 1: The three vinyl derivative molecules studied in the present work: (a) acrylamide (ACA), (b) acrylonitrile (ACN), and (c) acrolein (ACO). Labels of atoms in each molecule correspond to those employed in the text and tables. Figure also published in *J.Phys.Chem.C* 2018, 122, 27301–27313.

from the molecule to the substrate. Vibrational relaxation lifetimes of molecules adsorbed at metal surfaces have been measured to be in the range of a few picoseconds[71–73] or even longer.[74] The response of vibrationally excited adsorbed molecules on metals, and the energy relaxation mechanisms have been matter of study during the last decades.[75–79] Electron-hole pair excitations has been found to be one of the dominant channels of vibrational energy dissipation of chemisorbed molecules. Novko et al. have recently investigated[80] the early stage dynamics of excited carbon monoxide molecules adsorbed on Cu(100) unveiling the microscopic processes behind the vibrational spectroscopic changes induced by femtosecond laser pulses. In a recent work,[81] Ge et al. showed competition between two channels in the vibrational energy relaxation dynamics of rhenium based catalysts adsorbed on metal surfaces: intramolecular vibrational relaxation and electron-hole pair mechanisms were shown to occur in the same time scale.

In spite of the experimental and theoretical efforts many questions still remain open, such as the mechanisms of the vibrational relaxation of excited molecules in direct energy transfer to substrate vibrational modes (phonons), the influence of the anchorage, the presence of different functional groups in these mechanisms, and the behavior of highly vibrationally excited organic molecules chemisorbed on metal surfaces. We provide insight on these ques-

tions in this work by means of theoretical simulations based on Density Functional Theory (DFT) and *Ab Initio* Molecular Dynamics (AIMD). We present an exhaustive study of the adsorption of three vinyl-derivatives (acrylamide, ACA; acrylonitrile, ACN and acrolein, ACO) on a pristine Cu(111) surface. These molecules have a common skeleton (a terminal double C=C bond) and they differ in their substituents, which are able to conjugate with the vinyl group, thus changing the electron density distribution along the skeleton (see Fig. 1). The metallic character of the surface is correctly described due to the inclusion of Periodic Boundary Conditions (PBC) in the simulations, avoiding spurious quantization of the electron density due to the finite size of the system. The combination of DFT+PBC has been successfully used to study this kind of systems (see e.g.[12,82–90]). Weak interactions (such as Van der Waals forces), which have been proved to be crucial in the adsorption of organic molecules on metal surfaces,[12,87,89–94] are taken into account through the methodology developed by Dion et al.[95–97]

We have structured our work in three parts: (i) first we present a static study including adsorption energies and geometries, charge transfer and electronic structure; (ii) then, vibrational modes of the adsorbed molecules on the metal surface are presented, focussing mainly in the role of the interaction to understand frequencies shift with respect to the gas-phase; (iii) finally, *ab initio* molecular dynamics simulations on the highly-excited molecules (6 and 12 eV of internal energy) show energy dissipation dynamics, molecular cleavage processes and decomposition kinetics. All these results aim to provide insight for the future development of efficient heterogeneous catalysts and new catalytic strategies.

Computational details

Both, static and dynamic calculations, were performed with the Vienna Ab initio Simulation Package (VASP) software,[98,99] which is based in the Density Functional Theory (DFT) and take advantage of the Periodic Boundary Conditions (PBC), essential to account for

the periodicity of the system and thus to properly describe the metallic character of the surface. The optPBE functional[95–97,100] was chosen for this work, since it has been shown to provide accurate results for the interaction of organic molecules with metallic surfaces (see e.g.[2,12,101,102]). The interaction between ions and electrons is described by using the Projector Augmented Wave (PAW) pseudopotentials,[103,104] obtained from the VASP database. The electronic density is calculated with a plane-wave expansion, up to a kinetic energy of 750 eV for the static calculations. In the case of the molecular dynamics simulations, due to the higher computational effort, the cutoff was set to 500 eV, enough to converge the adsorption energies. We have used in all the calculations the same periodic supercell; it consists in a four-layer slab with 5×5 copper atoms in each of the directions that define the hexagonal (111) surface. A vacuum of 20 Å is included in the $z-$axis, direction perpendicular to the surface, in order to avoid the interaction with the closest replica and to let the system enough space to evolve in the molecular dynamics simulations. This supercell size has been shown to provide converged results.[12,88] The Brillouin zone was sampled by using the $\Gamma-$point in the optimization. Optimized geometries are used in single point calculations using a $\Gamma-$centered Monkhorst-Pack scheme[105] with a $3\times3\times1$ K-points sampling, in order to have more accurate adsorption energies. This methodology was previously used with success in,[12] with a typical error in adsorption energies smaller than $\sim$ 10 meV. To determine the partial occupancies, we have used the first-order Methfessel-Paxton scheme,[106] with a σ value of 0.2 eV. The electronic self-consistent convergence was set to 10^{-5} eV to have highly accurate energies and gradients. In the case of the molecular dynamics simulations, this value was set to 10^{-4} eV. For the convergence criteria in the geometry optimizations, we have imposed to all the Hellmann-Feynman forces to be lower to 5×10^{-3} eV/Å for the geometrical variables to be relaxed (x, y, z of all the atoms in the molecule and the z coordinate of the first layer of the slab).

Atomic charges have been computed by using the Quantum Theory of Atoms In Molecules (QTAIM).[107,108] For this purpose, and taking advantage of the numerical grid which VASP

uses to store the electron density, we have employed the code developed by Henkelman et al.[109–111] to perform the grid integration.

In order to characterize the surface-molecule interactions, we have also carried out a projected Density Of States (pDOS) analysis. To do this, we project the total Density Of States (DOS) on the different angular momenta of every atom inside the supercell. With all these contributions, one can easily determine which states contribute on each projection. This technique is useful to identify the molecular orbitals that are mixed with substrate states leading to molecule-metal interactions.

Vibrational frequencies have been evaluated under the harmonic approximation. In this case, we have performed a central difference calculation. Each degree of freedom of the molecule and the z coordinate of the atoms of the first metal layer are moved ± 0.015 Å from the equilibrium position in order to obtain the Hessian matrix. Then, the matrix is diagonalized and the normal modes (eigenvectors) and energies (eigenvalues) are obtained. We have benchmarked the vibrational results obtained with VASP using as reference those computed at the PBE/aug-cc-pVTZ level of theory for the neutral molecule in the gas phase using the Gaussian09 code.[112] The greater difference between both codes in stretching modes is of $\sim$16 cm^{-1} (C1-C2 stretching in acrolein).

For the *ab initio* molecular dynamics simulations, all the coordinates of the molecule and the first, second and third atomic metal layers were allowed to move. In each trajectory the initial excitation energy (6 and 12 eV) was randomly distributed among the nuclear coordinates of the molecule. These are the typical values of multiple bond dissociation energies (see e.g.[113]) We run several trajectories for each considered molecule and each excitation energy value and then statistics were performed on them (a total of 180 trajectories for molecules adsorbed on a metal surface, and 90 trajectories for molecules on the gas phase were run). To ensure adiabaticity in the simulations, the time step was set to 0.3 fs, and we propagated the trajectories up to $\sim$ 0.5 ps (those with excitation energy of 12 eV) or $\sim$1 ps (those with excitation energy of 6 eV). These simulations were performed in the microcanonical

ensemble.

Results and Discussion

Adsorption Geometries, Interaction Energies and Charge Transfer

In the search of molecular adsorption sites we have carried out a systematic exploration of the potential energy surface. To this we have selected as initial guess in the geometry optimization several structures. The choice was done by placing the molecule, whose geometry was pre-optimized in the gas phase, in a parallel orientation with respect to the surface and at a distance of $\sim$2 Å. Then, we scanned the relative orientation of the molecule with respect to the surface keeping the parallel orientation, using different rotational angles, and taking advantage of the high symmetry of the hexagonal surface. With this strategy we have selected one hundred initial geometries to optimize. During the optimization process, similar structures were discarded using geometrical and energetic criteria, i.e. when two of them lead a similar configuration (in a visual inspection) and with a relative energy between them smaller than 5 meV. We finally obtained six possible adsorption structures for acrylamide, four for acrylonitrile and two for acrolein, named hereafter ACA[1-6], ACN[1-4] and ACO[1-2] respectively. The high symmetry of the surface and the limited molecular anchorage sites are probably the responsible of the low number of structures found. Fig. 2 shows the geometry of the optimized structures and Table 1 the adsorption energy E_{ads} of these structures, defined as:

$$E_{ads} = E_{mol/surface} - (E_{mol} + E_{surface}) \quad (1)$$

where $E_{mol/surface}$ is the energy of the total system (molecule adsorbed on the surface), E_{mol} is the energy of the molecule without any interaction with the surface (optimized in the gas phase) and $E_{surface}$ is the energy of the pristine slab.

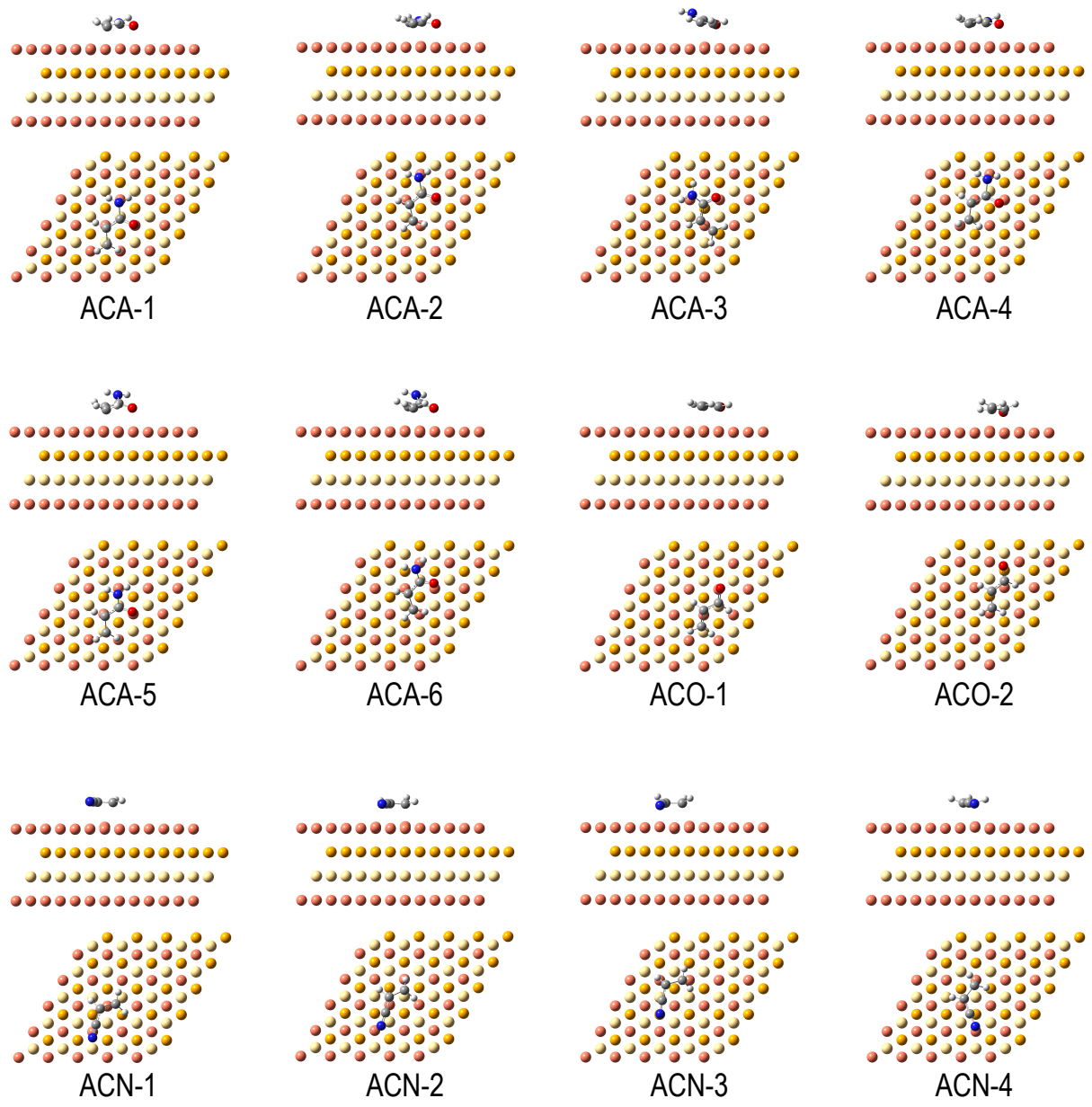

Figure 2: Top and side view of the minima found for acrylamide (ACA), acrylonitrile (ACN) and acrolein (ACO) adsorbed on a Cu(111) surface. Three colors for the different Cu layers are used.

In the obtained structures for the three studied molecules, the vinyl group plays a crucial role in the interaction with the surface. In a simple visual inspection, loss of planarity of the terminal CH_2 group is observed in all cases. This is the consequence of the strong interaction between the C atom and the surface which implies charge transfer and chemisorption, as we

Table 1: Adsorption energy E_{ads} of acrylamide (ACA), acrylonitrile (ACN) and acrolein (ACO) on a Cu(111) surface. Several structures were obtained for each molecule (see Fig. 2). Relative energy ΔE between the structures in each system. All values are in eV.

	E_{ads} (eV)	ΔE (eV)
ACA-1	-0.520	0.208
ACA-2	-0.477	0.251
ACA-3	-0.728	0.000
ACA-4	-0.466	0.262
ACA-5	-0.637	0.091
ACA-6	-0.569	0.159
ACN-1	-0.354	0.000
ACN-2	-0.145	0.208
ACN-3	-0.135	0.219
ACN-4	-0.271	0.083
ACO-1	-0.456	0.000
ACO-2	-0.442	0.014

will show below. It can be easily explained within the hybrid orbital model: charge transfer from the molecule to the surface leads to a change in hybridization in the terminal C atom from sp^2 in the gas phase to sp^3 in the adsorbed structure, forming a new chemical bond between the molecule and the surface (see the dihedral angles in Table 2). Indeed, in the energetically most favourable structure found for the three molecules (ACA-3, ACN-1 and ACO1) the terminal C=C bond lies on top of a Cu atom of the surface forming a $\eta^2 - \mathrm{Cu}$ bond, thus showing that the vinyl–surface interaction is the main anchorage point and the key stabilizing factor. In the case of Cu(100) we also found that the most stable structure of the considered vinyl-derivatives are those in which the double C=C bond is on top of a Cu atom of the surface.[12]

The adsorption structures that we have found for ACA show in common a direct, on top, interaction between the oxygen atom of the molecule and a Cu atom of the surface, with relative energies between them of up to $\sim$ 260 meV. In ACA-1, ACA-2 and ACA-4 we also distinguish direct interaction between the N atom and a Cu atom of the surface ($\mathrm{N}\rightarrow\mathrm{Cu_{top}}$); in these cases the hybridization also changes in the N atom from sp^2 to sp^3 and the geometry is accordingly distorted. However in ACA-3, ACA-4, ACA-5 and ACA-6

planarity in the amide group is observed; in these cases hybridization is not altered and the resonant amide structure O-C=NH_2 is preserved. The geometrical changes upon adsorption are also reflected in the electronic structure and are discussed below.

In the case of ACN, the cyano and vinyl groups change the position in each adsorption geometry (on top of a Cu atom and on hollow between Cu atoms in the surface), showing differences in the adsorption energy of up to $\sim$ 220 meV. ACO-1 and ACO-2 are nearly degenerated (ΔE = 14 meV). Interestingly, the less stable one (ACA-2) shows a stronger interaction between the O atom and the Cu one (the distance between O and the surface is 1.8 Å; while in ACA-1 is 2.2 Å) and presents a higher distortion of the molecule upon adsorption (e.g. the dihedral angle H-C-C-C is 146° in ACO-2 and 163° in ACO-1, being planar in the gas phase 180°). It suggests that in ACO-2 the deformation energy (with respect to the gas phase structure) is countered with the adsorption one, but not enough to become the most stable conformation.

We now analyze in more detail the nature of the molecule–surface interaction focusing on the most stable structure of each studied system (ACA-3, ACN-1 and ACO-1). The adsorption leads to charge transfer from the surface to the molecule in the three cases (see Table 2). However, no relation between the charge transfer and the adsorption energy is observed. The highest charge transfer from the surface to the molecule is observed in acrolein, followed by acrylonitrile and acrylamide. We obtained similar trends and absolute values in the adsorption of the same molecules on the Cu(100) surface,[12] which points out that the charge transfer does not depend on the crystal orientation but on its chemical composition and on the adsorbed organic molecule.

Charge transfer can be further studied by analysing the change in the spatial redistribution of the electronic density upon adsorption, which is defined as:

$$\Delta\rho = \rho_{molecule/surface} - (\rho_{molecule} + \rho_{surface}) \tag{2}$$

Table 2: Most relevant C−C distances (in Å), dihedral $H-C2-C3-H$ angles in adsorption (in degrees, hydrogen atoms in *trans*) and transferred charge from the surface to the molecule (in atomic units) of the most stable minima found for acrylamide, acrylonitrile and acrolein adsorbed on a Cu(111) surface after geometry optimization. Gas phase distances are also included for comparison.

	$C1-C2$		$C2-C3$		$H-C2-C3-H$	Δq
	Gas phase	Adsorbed	Gas phase	Adsorbed	Dihedral angle	
ACA-3	1.497	1.462	1.337	1.414	153.6	-0.224
ACN-1	1.427	1.416	1.342	1.411	157.7	-0.244
ACO-1	1.473	1.444	1.342	1.412	161.6	-0.388

where $\rho_{molecule/surface}$ is the electronic density of the whole system, and $\rho_{molecule}$ and $\rho_{surface}$ are the electronic densities of the molecule and surface computed keeping the adsorption geometry. Fig. 3 shows that the charge is mainly transferred to the vinyl group in the three molecules, i.e. from the surface to the lowest unoccupied molecular orbital (LUMO), which has π^* character. Therefore, the π system in the molecule becomes more homogeneous due to the adsorption and this is reflected on changes in the geometry. Indeed, the C1-C2 bond (single C-C bond in gas phase) is shortened, while the C2-C3 bond (double C=C bond in the gas phase) lengthens, as can be observed in Table 2. The distortion of the molecular skeleton upon adsorption is the direct consequence of the stronger electronic delocalization. The distortion in the molecular geometry, specially those changes in the C-C bond distances and the loss of planarity in the vinyl group, together with the charge transfer results, confirm the nature of the molecule–surface interaction as chemisorption. As has been shown before for vinyl derivatives adsorbed on Cu(100),[12] the depletion of electron density in regions where there is no nodal plane in the π system and the gain in the LUMO orbital is explained in terms of a simple chemical picture: electron donation from the π orbital of the molecule to the surface and backdonation from the surface to the π^* orbital of the molecule ($\pi-$backbonding). This phenomenon was also observed in other molecules of different nature adsorbed on metal surfaces[59,114–118]

In order to get a deeper information on the changes in the electronic structure upon adsorption and on the nature of the interaction, we have analyzed the density of states

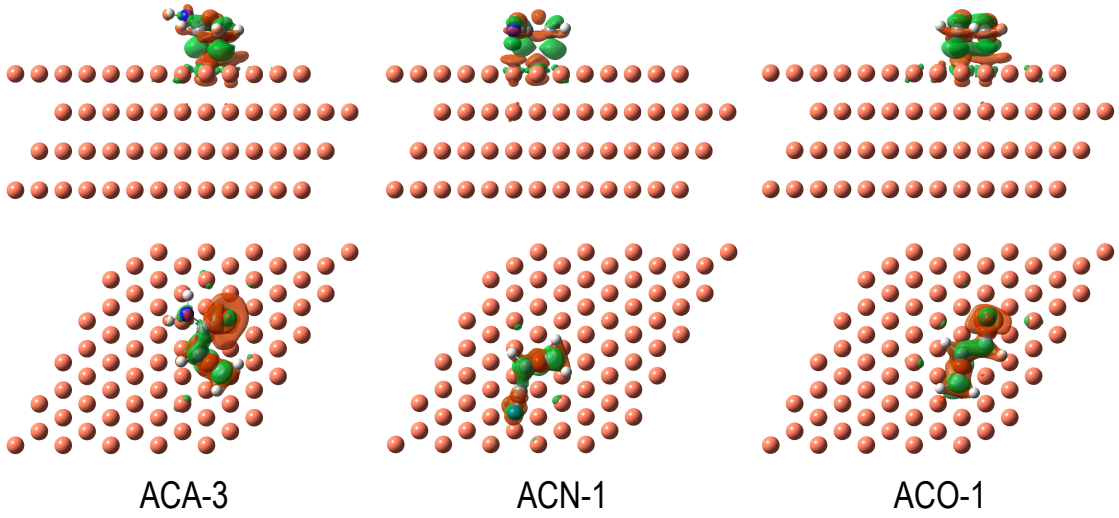

Figure 3: Change in the electronic density upon adsorption ($\Delta\rho$, isovalue=0.02) for the most stable adsorption structures of the three vinyl derivatives on Cu(111) surface. Green shows possitive $\Delta\rho$ and reddish orange negative $\Delta\rho$. All the Cu atoms in this figure are shown in the same color.

projected on molecular states: projected Density Of States (pDOS). They are shown, for the most stable adsorption conformer, in Fig. 4. Due to the different Fermi levels of the molecule and surface separately, when they interact, there is an energy alignment which induces a charge transfer from the metal to the organic molecule.[21,119] For this reason, since the molecule has a partial negative charge, its nuclei have an extra screening, shifting its electronic levels. This is a common feature of all the molecular states, regardless of their symmetry. As we have explained, charge transfer takes place mainly through the π orbitals of the molecule; due to their spatial orientation, the overlap with the metal states is more favorable and thus, these orbitals are able to mix more efficiently with the surface. This is clearly appreciated in the pDOS: the π states (in red) are the ones that have a higher change upon molecular adsorption: they are the only molecular states that do not keep their previous identity showing a larger broadening and higher energy shift. This observation confirms the nature of the chemical interaction: donation from the occupied lone pair and π orbitals of the molecule to the surface and backdonation from the surface to the π^* orbital of the molecule ($\pi-$backbonding).

Table 3: Wavenumbers (in cm^{-1}) associated to the stretching modes of the acrylamide (ACA), acrylonitrile (ACN) and acrolein (ACO), in the gas phase (neutral and anion) and in the most stable adsorption geometry on Cu(111).[(a)]In the case of the acrolein, the frequency at 910.92 cm^{-1} is strongly coupled with other mode at 1149.93 cm^{-1}. Although Hamada et al.[120] assigned the C1-C2 stretching to this band (1158 cm^{-1} in their work), an analysis of the contributions of the normal modes shows that this internal coordinate contributes approximately equal to both bands. In this work we propose this new assignment since it is consistent with the other vinyl-derivatives and with the shift after the adsorption. Frequencies of anionic molecules in the gas phase have been computed with Gaussian09.[112]

stretching mode	Gas Phase		Molecule/Cu(111)
ν	ACA neutral	ACA anion	ACA-3
NH_2 asymmetric	3627.01	3477.66	3578.58
NH_2 symmetric	3494.81	3356.24	3448.05
CH_2 asymmetric	3166.46	3155.30	3142.67
CH_2 symmetric	3082.50	3069.88	3053.34
C-H	3065.00	3039.22	3079.02
C=O	1680.84	1586.16	1483.68
C2=C3	1624.43	1468.19	1417.15
C-N	1256.36	1257.72	1274.84
C1-C2	796.87	813.85	1383.82
ν	ACN neutral	ACN anion	ACN-1
CH_2 asymmetric	3182.71	3162.84	3167.93
C-H	3101.47	3060.99	3087.59
CH_2 symmetric	3086.79	3071.03	3074.74
C≡N	2253.28	2078.32	2094.58
C2=C3	1613.95	1454.19	1455.07
C1-C2	871.42	866.63	1350.37
ν	ACO neutral	ACO anion	ACO-1
CH_2 asymmetric	3159.48	3127.58	3143.39
C-H (vinyl)	3100.49	3020.88	3052.93
CH_2 symmetric	3067.72	3045.11	3047.44
C-H (aldehyde)	2790.37	2682.81	2818.41
C=O	1688.45	1466.86	1427.86
C2=C3	1618.60	1466.86	1457.79
C1-C2	910.92[(a)]	1197.22	1321.07

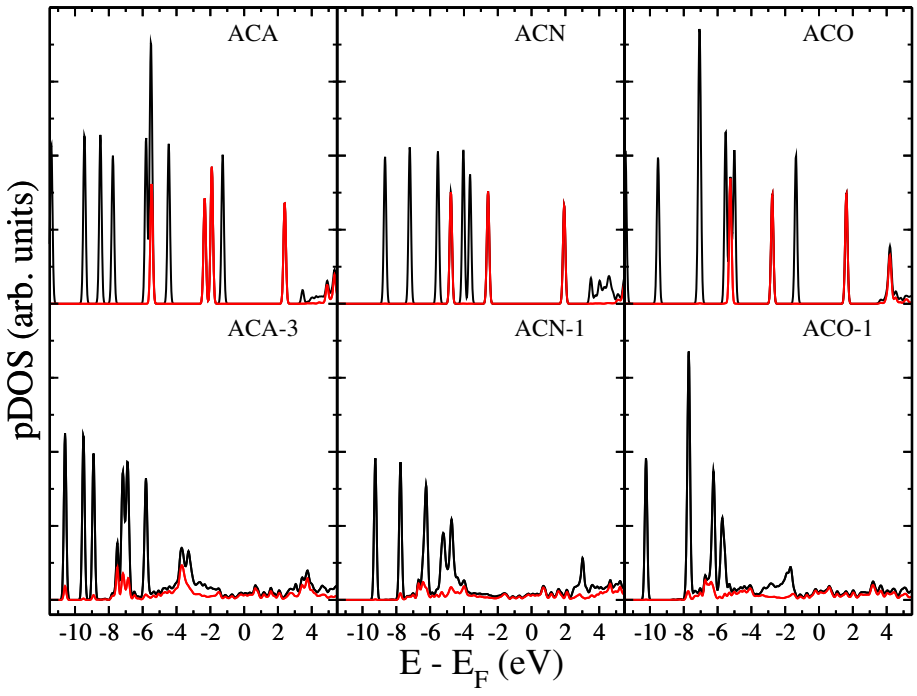

Figure 4: Density Of States projected on the atoms of the adsorbed molecules. Results of the molecule far from the slab, non interacting with the surface, is also shown for comparison - upper curves in each panel. Black curve: total pDOS; Red curve: pz-projection, which allows to identify the π contribution to the pDOS.

Vibrational Frequencies

We now present how the molecule-surface interaction, characterized in the previous section, influences the vibrational properties of the studied molecules. This is a first step towards understanding their behaviour upon thermal excitation (see next section). In particular, we have computed the harmonic vibrational frequencies of the most stable adsorption structure for each vinyl-derivative. We present in Table 3 the computed frequencies of the most relevant vibrational modes. For comparison, vibrational frequencies of the same modes for the neutral and the anion molecules in the gas phase are also shown.

The three vinyl-derivatives exhibit the same trends after the adsorption. The C1-C2 stretching mode increases its frequency in several hundreds of cm^{-1} in the adsorbed structures, which indicates a stronger bond. On the other hand, the double C2=C3 bond decreases its characteristic frequency from $\sim$ 1620 to $\sim$ 1460 cm^{-1}. In this way, in the adsorbed

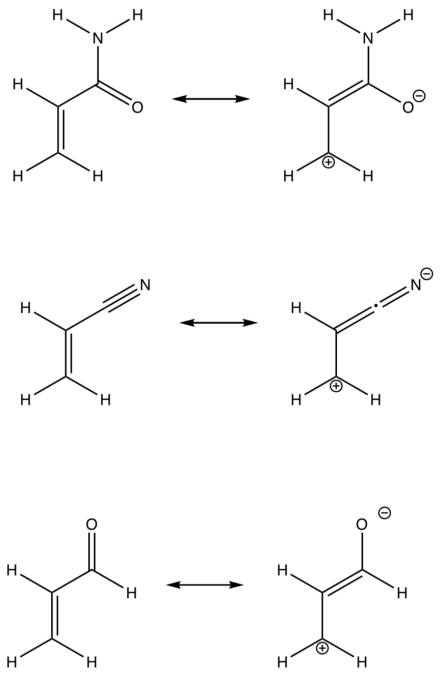

Figure 5: Resonance forms of acrylamide (up), acrylonitrile (middle) and acrolein (down). The two relevant structures for the discussion are shown for each molecule.

molecules the difference between both frequencies (C1-C2 and C2-C3 stretching modes) is much smaller than in the gas phase. This is the consequence of the higher electron delocalization in the molecular skeleton, as stated in the previous section. Accordingly, changes in the C1-C2 and C2-C3 bond lengths in the adsorbed structures lead to very similar distances after the adsorption (1.4 Å). Also, both the symmetric and antisymmetric $\nu(CH_2)$ frequencies are red-shifted, which is consistent with the change of hybridization of the terminal C3 atom due to the interaction with the surface: it adopts a partial sp^3 character and they decrease in ~ 20 cm^{-1}.

In the substituent groups (C=O for ACO, C≡N for ACN, and NH_2C=O for ACA) variations in the frequencies of the stretching modes can be also explained in terms of charge transfer and molecular chemisorption to the metal surface. The amide group of acrylamide

has an important contribution to the Lewis structure in which the electron lone pair of the nitrogen atom migrates to form a double bond with the carbon, thus shifting the pair in the C=O to the oxygen atom. In this resonant form, a partial negative charge is placed on the oxygen atom (see Fig. 5). In the adsorption a non negligible part of the transferred charge is accommodated on the oxygen atom (see $\Delta\rho$ in Fig. 3) thus decreasing the weight of this resonant structure. Consequently, the lone pair of the nitrogen does not participate on the resonant structure and is thus available to link the molecule to the surface. The N atom adopts a sp^3 character, causing a red-shifting in both symmetric and antisymmetric $\nu(NH_2)$ stretching frequencies. In addition, since larger electron density is hosted in the molecule, the oxygen atom does not form anymore a pure double C=O bond and consequently the corresponding stretching frequency is also red-shifted.

In acrylonitrile, the C $\equiv$ N bond in the cyano group becomes more labile in the adsorption because (i) part of the electron density initially located on this bond is now participating in the linkage with the surface ($\pi \rightarrow$ Cu donation) and (ii) the extra transferred charge populates the π^* orbital (Cu $\rightarrow \pi^*$ backdonation).[12] Thus, red-shifting is also observed in the stretching frequency of this bond, as it has been shown experimentally.[121]

Finally, the acrolein has two internal stretching modes: the double C=O bond, which behaves as the CO bond of the amide group (red-shift due to the adsorption) and the C-H bond of the aldehyde. This last frequency is blue-shifted after the interaction with the surface. This change can be also explained due to the high electron transfer from the metal to the molecule. An internal rearrangement of the electron density is observed and although the molecule hosts globally 0.39 e^- from the surface, locally in the C1-C2 bond 0.46 e^- is distributed. The charge excess strengthens the bond and therefore it becomes shorter, causing an increase in the frequency of the $\nu(C1-H)$ stretching mode.

Although changes observed in some modes upon adsorption point in a similar direction to those in the negatively-charged molecules in the gas phase, the trends in a few modes follow an opposite behavior [$\nu(C-H)$ in ACA, $\nu(C1-C2)$ in ACN and $\nu(C-H_{aldehyde})$ in ACO].

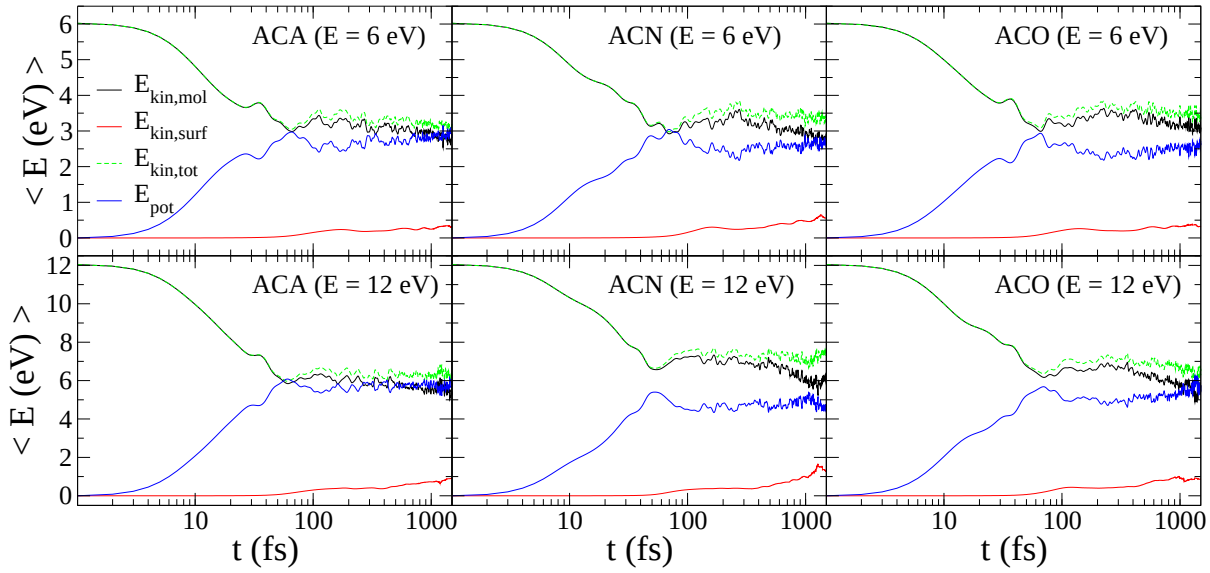

Figure 6: Energy exchange among the kinetic energy of the atoms in the molecule ($E_{kin,mol}$), kinetic energy of the atoms in the surface ($E_{kin,surf}$), total kinetic energy ($E_{kin,tot}$) and potetial energy (E_{pot}), as a function of the time in the *ab initio* molecular dynamics simulations. Each energy contribution has been averaged in time over the trajectories. Acrylamide (ACA), acrylonitrile (ACN) and acrolein (ACO) with 6 and 12 eV of initial excitation energy have been considered.

This indicates that the new vibrational leves are affected not only by charge transfer effects, but also by the covalent interactions with the surface that strongly anchor the molecule, thus hindering certain atomic displacements.

Ab initio Molecular Dynamics

Finally we have studied the behavior of excited vinyl derivatives (ACA, ACN, ACO) adsorbed on a Cu(111) surface by means of *ab initio* molecular dynamics (AIMD). To this we have computed several trajectories for each system assuming two values of excitation energy (E^* = 6 and 12 eV) randomly distributed among the nuclear degrees of freedom of atoms in the molecule. During the propagation we allow the movement of all the atoms (except the last layer inside the metal bulk). For comparison, AIMD simulations on the molecules in gas phase were also carried out.

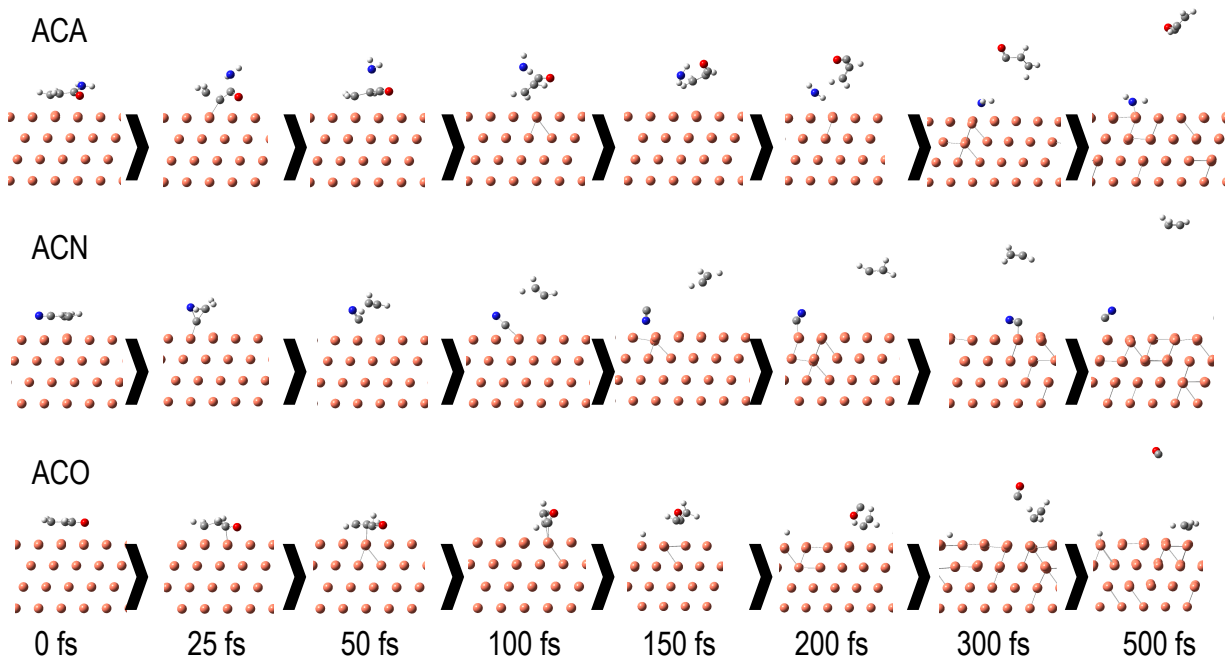

Figure 7: Snapshots of *ab initio* molecular dynamics trajectories for acrylamide (ACA), acrylonitrile (ACN) and acrolein (ACO) with 12 eV of initial excitation energy. The selected trajectories shows molecular breaking leading to (i) $NH_{2(Ads)}$ + $CHOCH_2$ for ACA; (ii) $CN_{(Ads)}$ + CH_2CH for ACN; (iii) $H_{(Ads)}$ + $CH_2CH_{(Ads)}$ + CO for ACO

We first analyze the excitation energy distribution and transfer dynamics. Fig. 6 shows the energy decomposition as a function of the time: potential energy, kinetic energy in atoms of the molecule, kinetic energy in atoms of the metal and total kinetic energy. Each curve corresponds to an average over all the computed trajectories (with fluctuations of $\sim 7-25\%$). In all cases (regardless the molecule or the excitation energy) a similar behavior is observed: During the first $\sim$ 20 fs, the excitation energy is gradually transferred from kinetic energy in the molecule to potential energy; i.e the energy is very rapidly redistributed and the system suffers strong deformations from its departure point in the optimized geometry. Then, it reaches a pseudo-equilibrium in which $\sim$ 50% of the kinetic energy has been transferred to potential energy. From this point on, the kinetic energy remaining in the atoms of the molecule is slightly transferred into kinetic energy of the atoms in the surface. The highly-excited molecules evolve breaking bonds (molecule-surface or intramolecular bonds) during the first femtoseconds in the propagation and transfer of thermal energy from the molecule

to the surface is only effective when the atoms of the molecule have cooled down. The main reason is the difference in mass between them: since the copper atoms on the surface are (at least) four times heavier than the atoms of the molecule inelastic collisions are only effective at low velocity; that is, from the remaining atoms of the molecule that still interact with the substrate, the transfer of momentum to the metal atoms takes place in a kind of friction process. A deeper analysis on the movements of Cu atoms reveals that the coordinates in these atoms are frozen during the first part of the propagation, even if they are allowed to move; only when the potential energy has reached a maximum the Cu atoms begin to move from their original positions. This result indicates that all the potential energy gain is in the form of molecular deformation or desorption.

We now focus on the chemical processes taking place after excitation. To this we analyze the final products obtained after the molecular dynamics propagation. We first analyze the three main processes that we have observed:

- Adsorption: The molecule is still interacting with the surface. Most probably it has been moved from its original adsorption site. In this process, isomerization can be also observed.

- Desorption: The molecule is desorbed and does not interact with the surface any more. In this process, isomerization is also observed.

- Break: Bonds in the molecule suffer cleavage producing two or more fragments (see examples of trajectories following this kind of dynamics in Fig. 7).

Fig. 8 shows the probability of these processes in the three studied molecules (molecular breaking in the gas phase with $E^* = 12$ eV is also shown for comparison). When the molecule breaks, the produced fragments can desorb or stay interacting with the surface (part of them or all of them). This information is also shown in the figure. The general trends are similar in the three studied molecules (although percentages differ from one to other). The probability of finding trajectories with molecular adsorption decreases with the energy, from $\sim$ 70%

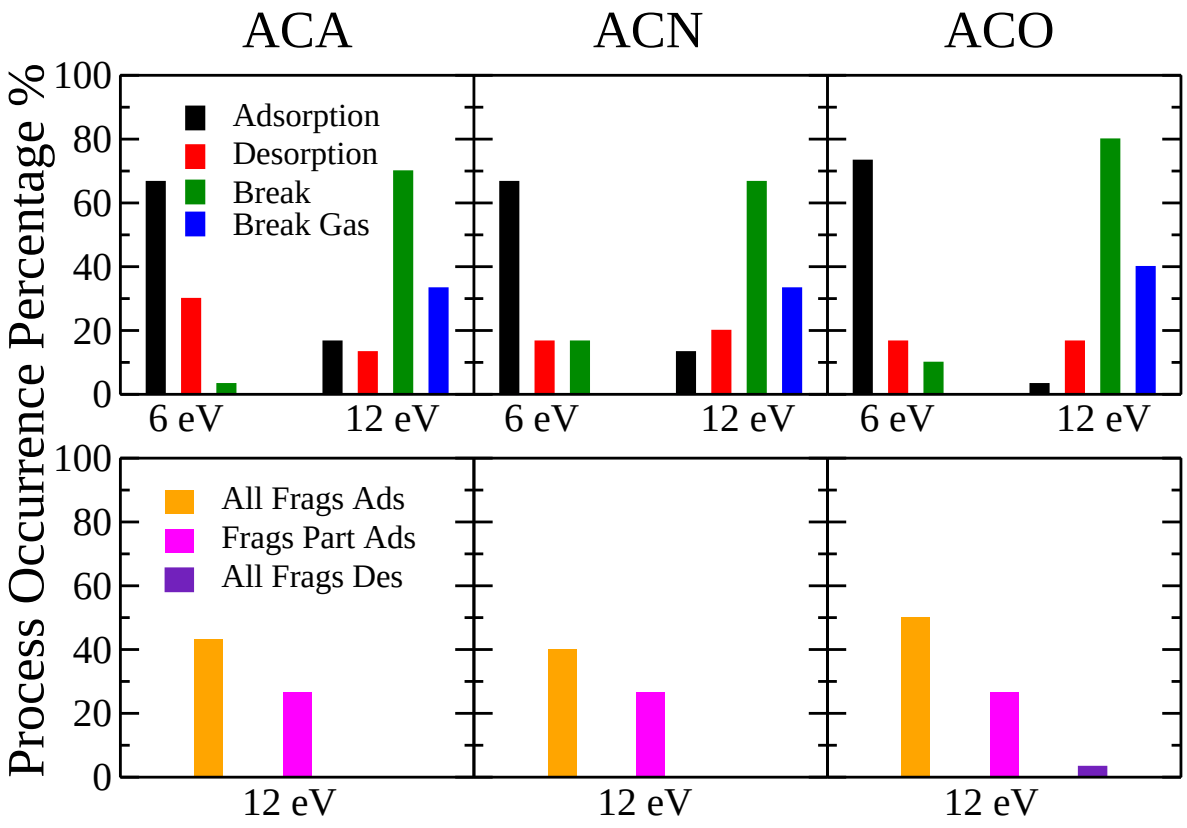

Figure 8: Percentage of the processes occurrence obtained in the molecular dynamics for the three studied molecules acrylamide (ACA), acrylonitrile (ACN) and acrolein (ACO). Upper panels (excitation energy 6 and 12 eV): The molecule remains adsorbed (Adsorption); the molecule desorbs (Desorption); the molecule is broken (Break). Lower panels (excitation energy 12 eV): when the molecule is broken, all produced fragments remain adsorbed (All Frags Ads), all produced fragments desorb (All Frags Des), part of the fragments remains adsorbed and the rest desorb (Frags Part Ads). In the upper panels the results for the molecular breaking percentage of the molecules in gas phase at 12 eV are also shown.

at 6 eV to $\sim$ 10% at 12 eV. Acrylamide shows larger desorption at 6 eV than at 12 eV (most probably because we found much less molecular breaking at 6eV in comparison with 12 eV). In acrylonitrile and acrolein similar amount of molecular desorption is found at 6 and 12 eV ($\sim 15-20\%$). Molecular breaking is the dominant process at 12 eV in the three molecules adsorbed with the surface ($\sim 70-80\%$). It is worth to stress that the amount of molecular breaking observed in the molecules in gas phase with the same excitation energy (12 eV) is half of the observed in the adsorbed systems. Even if part of the excitation energy is transferred to the metal surface, the probability of finding molecular fragments is much larger. The reason is that the interaction of the molecule with the metal surface weakens the bonds between atoms in the molecule. In particular, the charge transferred in the chemisorption is mainly located on the LUMO orbital of the molecule, with a strong π^* antibonding character: larger π conjugation but making C=C bonds much more labile. We observe larger probability of molecular breaking in the surface when all the produced fragments remain adsorbed on the substrate. A negligible amount of desorption of all the produced fragments is appreciated. But the catalytic effect of the metal surface is not only observed in the larger amount of fragmentation produced when the molecule is interacting with the substrate, but also in a much wider spectrum of produced fragments (see Tables 4, 5 and 6). Some of the observed fragments in the gas phase are not present in the adsorbed systems, but a much richer fragmentation behavior is observed. In general:

- Atomic hydrogen is widely observed in the adsorbed molecules while almost negligible in the gas phase.

- In gas phase stable molecular species are mainly produced, such as ethylene $H_2C = CH_2$, acetylene $HC \equiv CH$, molecular hydrogen H_2, hydrogen cyanide HCN, or carbon monoxide CO.

- The vynil moiety C_2H_3, coming from a direct cleavage of the central C-C bond is one of the most observed fragments. Since the charge transferred is accommodated

on the LUMO it increases the π delocalization reinforcing the central C-C bond; this strengthening is reflected in the less amount of the vinyl fragment observed in the adsorbed molecules.

In particular for each molecule:

- In acrylamide NH_2 is much more observed in the adsorbed molecule being the dominant fragment (50%).
- In acrylonitrile HCN is the most abundant fragment in gas phase and it is not observed on the adsorbed molecule, where the CN fragment is largely the dominant one (60%).
- In acrolein HCO and C_2H_3 are common fragments in gas phase. While C_2H_3 is also one of the most abundant in the adsorbed molecule, HCO almost disappears being now CO much more probable.

Conclusions

In summary, we have presented a deep theoretical study of organic-metal interfaces, focussing on the electronic properties and thermal stability of potential candidates for composite hybrid materials. In particular we have performed density functional theory (DFT) simulations of the vinyl derivative polymer precursors acrylamide, acrylonitrile and acrolein, interacting on a pristine Cu(111) surface. The modeling highlighted anchoring mechanisms and the preferred arrangement of the molecules at the surface. Interestingly, the vinyl group acts as the binding site and the functional groups in each molecule drive the relative adsorption orientation. Linkage with the surface can be explained with a simple chemical picture: $\pi \rightarrow$ Cu donation and Cu $\rightarrow \pi^*$ backdonation. Changes in the electronic structure associated to this kind of interaction show stronger electronic delocalization and consequently distortion of the molecular skeleton. Molecular anchoring (through the vinyl group) and structural changes (bond elongations and dihedral angles modifications upon adsorption) suggest the

possibility of controlled polymerization in given crystal orientations. The *ab initio* molecular dynamics simulations have shown a very efficient energy redistribution (shared between the kinetic energy of atoms in the molecule, in the surface and potential energy in a short time of $\sim$ 100 fs). Molecular decomposition shows a much more varied spectrum when the molecule is adsorbed on the surface and, notably, a catalytic effect with a larger amount of fragmentation with respect to molecules in the gas phase. These findings may help achieve a deeper comprehension of the properties of ultra-thin organic coating of metal surfaces, a promising two dimensional kind of hybrid material with potential applications in many areas.

Table 4: Percentage of *ab initio* molecular dynamics trajectories where the corresponding fragment of the acrylamide (ACA) molecule is produced. Results when the molecule is adsorbed on Cu(111) and for the molecule in gas phase are given, both with initial excitation energy 12 eV.

Fragment	ACA/Cu(111)	Gas Phase
H	23.33	–
ACA-H	3.33	–
NH_2	50.00	13.33
ACA-NH_2	13.33	3.33
CH_2	13.33	–
ACA-CH_2	0.00	–
O	10.00	–
ACA-O	3.33	–
C_2H_3	16.67	20.00
C_2H_2	13.33	–
CO	26.67	10.00
OC_2H	10.00	–
NH_2C_2H	3.33	–
NHC_3H_3	3.33	–
$OCNH_2$	6.67	–
CH	3.33	–
NH_2COH	–	3.33
NH_2CO	–	10.00
CH_2CH_2	–	3.33
CHCH	–	3.33
HNCO	–	3.33

Table 5: Percentage of *ab initio* molecular dynamics trajectories where the corresponding fragment of the acrylonitrile (ACN) molecule is produced. Results when the molecule is adsorbed on Cu(111) and for the molecule in gas phase are given, both with initial excitation energy 12 eV.

Fragment	ACN/Cu(111)	Gas Phase
H	33.33	–
ACN-H	6.67	–
C_2H_2	23.33	3.33
CN	60.00	13.33
C_2H_3	30.00	13.33
CH	3.33	–
CH_2	6.67	–
C	3.33	–
CHCH	–	13.33
HCN	–	16.67

Table 6: Percentage of *ab initio* molecular dynamics trajectories where the corresponding fragment of the acrolein (ACO) molecule is produced. Results when the molecule is adsorbed on Cu(111) and for the molecule in gas phase are given, both with initial excitation energy 12 eV.

Fragment	ACO/Cu(111)	Gas Phase
H	56.67	3.33
ACO-H	3.33	–
CH_2	6.67	–
ACO-CH_2	3.33	–
CO	36.67	13.33
C_2H_2	10.00	3.33
C_2H_3	33.33	30.00
CH	6.67	–
OC_2H_2	3.33	–
O	13.33	–
CH_2CCH_2	3.33	–
OH	6.67	–
C_3H_3	10.00	–
OCHCCH	3.33	–
C_2H	3.33	–
C_3H_2	3.33	–
$OCCH_2$	3.33	–
CHO	6.67	–
CHCH	–	6.67
HCO	–	26.67
H_2	–	6.67

Acknowledgement

We acknowledge the generous allocation of computer time at the Centro de Computación Científica at the Universidad Autonóma de Madrid (CCC-UAM) and the Red Española de Supercomputación (RES). This work was partially supported by the project CTQ2016-76061-P of the Spanish Ministerio de Economía y Competitividad (MINECO). F.A.G. acknowledges the FPI grant associated with the project CTQ2013-43698-P (MINECO). Financial support from the MINECO through the "María de Maeztu" Program for Units of Excellence in R&D (MDM-2014-0377) is also acknowledged. The authors gratefully acknowledge inspiring and fruitful discussions with Dr. Octavio González del Moral.

References

(1) Rosei, F.; Schunack, M.; Naitoh, Y.; Jiang, P.; Gourdon, A.; Laegsgaard, E.; Stensgaard, I.; Joachim, C.; Besenbacher, F. Properties of large organic molecules on metal surfaces. *Prog. Surf. Sci.* **2003**, *71*, 95 – 146, Proceedings of the IXth Symposium on Surface Physics, Trest Castle 2002.

(2) Liu, W.; Tkatchenko, A.; Scheffler, M. Modeling adsorption and reactions of organic molecules at metal surfaces. *Acc. Chem. Res.* **2014**, *47*, 3369–3377.

(3) Otero, R.; de Parga, A. V.; Gallego, J. Electronic, structural and chemical effects of charge-transfer at organic/inorganic interfaces. *Surf. Sci. Rep.* **2017**, *72*, 105 – 145.

(4) Brillson, L. *Surfaces and Interfaces of Electronic Materials*; Wiley - IEEE; Wiley, 2012.

(5) Koch, N.; Ueno, N.; Wee, A. *The Molecule-Metal Interface*; Wiley, 2013.

(6) Wandelt, K. *Encyclopedia of interfacial chemistry: Surface science and electrochemistry*; Elsevier Science, 2018.

(7) Hammer, B.; Nørskov, J. K. Why gold is the noblest of all the metals. *Nature* **1995**, *376*, 238.

(8) Hammer, B.; Nørskov, J. Electronic factors determining the reactivity of metal surfaces. *Surface Science* **1995**, *343*, 211 – 220.

(9) Hammer, B.; Morikawa, Y.; Nørskov, J. K. CO chemisorption at metal surfaces and overlayers. *Phys. Rev. Lett.* **1996**, *76*, 2141–2144.

(10) Hammer, B.; Nørskov, J. *Impact of surface science on catalysis*; Advances in Catalysis; Academic Press, 2000; Vol. 45; pp 71 – 129.

(11) Nilsson, A.; Pettersson, L. G.; Nørskov, J. K. In *Chemical bonding at surfaces and interfaces*; Nilsson, A., Pettersson, L. G., Nørskov, J. K., Eds.; Elsevier: Amsterdam, 2008; pp xi – xii.

(12) Aguilar-Galindo, F.; Díaz-Tendero, S. Theoretical insights into vinyl derivatives adsorption on a Cu(100) surface. *J. Phys. Chem. C* **2018**, *122*, 27301–27313.

(13) Armbrust, N.; Schiller, F.; Güdde, J.; Höfer, U. Model potential for the description of metal/organic interface states. *Sci. Rep.-UK* **2017**, *7*, 46561.

(14) Chen, S.; Zhao, Z.; Liu, H. Charge transport at the metal-organic interface. *Ann. Rev. Phys. Chem.* **2013**, *64*, 221–245.

(15) Scott, J. C. Metal-organic interface and charge injection in organic electronic devices. *J. Vac. Sci. Technol. A* **2003**, *21*, 521–531.

(16) Hwang, J.; Wan, A.; Kahn, A. Energetics of metal-organic interfaces: New experiments and assessment of the field. *Mat. Sci. Eng. R* **2009**, *64*, 1 – 31.

(17) Zaworotko, M. J. A reversible step forward. *Nat. Chem.* **2009**, *1*, 267.

(18) Furukawa, H.; Cordova, K. E.; O'Keeffe, M.; Yaghi, O. M. The chemistry and applications of metal-organic frameworks. *Science* **2013**, *341*.

(19) Zhou, H.-C.; Long, J. R.; Yaghi, O. M. Introduction to metal-organic frameworks. *Chem. Rev.* **2012**, *112*, 673–674.

(20) Sánchez, C.; Julian, B.; Belleville, P.; Popall, M. Applications of hybrid organic-inorganic nanocomposites. *J. Mater. Chem.* **2005**, *15*, 3559–3592.

(21) Ishii, H.; Sugiyama, K.; Ito, E.; Seki, K. Energy level alignment and interfacial electronic structures at organic/metal and organic/organic interfaces. *Adv. Mater.* **1999**, *11*, 605–625.

(22) Ferey, G. Hybrid porous solids: past, present, future. *Chem. Soc. Rev.* **2008**, *37*, 191–214.

(23) Yu, G.; Gao, J.; Hummelen, J. C.; Wudl, F.; Heeger, A. J. Polymer photovoltaic cells: enhanced efficiencies via a network of internal donor-acceptor heterojunctions. *Science* **1995**, *270*, 1789–1791.

(24) Günes, S.; Neugebauer, H.; Sariciftci, N. S. Conjugated polymer-based organic solar cells. *Chem. Rev.* **2007**, *107*, 1324–1338.

(25) Tang, C. W. Two-layer organic photovoltaic cell. *Appl. Phys. Lett.* **1986**, *48*, 183–185.

(26) Grätzel, M. Dye-sensitized solar cells. *J. Photoch. PhotoBio. C* **2003**, *4*, 145 – 153.

(27) Saragi, T. P. I.; Spehr, T.; Siebert, A.; Fuhrmann-Lieker, T.; Salbeck, J. Spiro compounds for organic optoelectronics. *Chem. Rev.* **2007**, *107*, 1011–1065.

(28) Shekhah, O.; Liu, J.; Fischer, R. A.; Woll, C. MOF thin films: existing and future applications. *Chem. Soc. Rev.* **2011**, *40*, 1081–1106.

(29) Choy, K. Chemical vapour deposition of coatings. *Prog. Mat. Sci.* **2003**, *48*, 57 – 170.

(30) Sirringhaus, H.; Tessler, N.; Friend, R. H. Integrated optoelectronic devices based on conjugated polymers. *Science* **1998**, *280*, 1741–1744.

(31) Rogers, J. A.; Someya, T.; Huang, Y. Materials and mechanics for stretchable electronics. *Science* **2010**, *327*, 1603–1607.

(32) Law, M.; Greene, L. E.; Johnson, J. C.; Saykally, R.; Yang, P. Nanowire dye-sensitized solar cells. *Nat. Mater.* **2005**, *4*, 455.

(33) Hagfeldt, A.; Boschloo, G.; Sun, L.; Kloo, L.; Pettersson, H. Dye-sensitized solar cells. *Chem. Rev.* **2010**, *110*, 6595–6663.

(34) Bogani, L.; Wernsdorfer, W. Molecular spintronics using single-molecule magnets. *Nat. Mater.* **2008**, *7*, 179.

(35) Rocha, A. R.; Garcia-Suarez, V. M.; Bailey, S. W.; Lambert, C. J.; Ferrer, J.; Sanvito, S. Towards molecular spintronics. *Nat. Mater.* **2005**, *4*, 335.

(36) Sanvito, S. Molecular spintronics. *Chem. Soc. Rev.* **2011**, *40*, 3336–3355.

(37) Mannini, M.; Pineider, F.; Sainctavit, P.; Danieli, C.; Otero, E.; Sciancalepore, C.; Talarico, A. M.; Arrio, M.-A.; Cornia, A.; Gatteschi, D.; Sessoli, R. Magnetic memory of a single-molecule quantum magnet wired to a gold surface. *Nat. Mater.* **2009**, *8*, 194.

(38) Gray, J.; Luan, B. Protective coatings on magnesium and its alloys - a critical review. *J. Alloy. Compd.* **2002**, *336*, 88 – 113.

(39) Huber, D. L. Synthesis, properties, and applications of iron nanoparticles. *Small* **2005**, *1*, 482–501.

(40) Chung, I.; Lee, B.; He, J.; Chang, R. P. H.; Kanatzidis, M. G. All-solid-state dye-sensitized solar cells with high efficiency. *Nature* **2012**, *485*, 486.

(41) Hakkinen, H. The gold-sulfur interface at the nanoscale. *Nat. Chem.* **2012**, *4*, 443.

(42) Nørskov, J.; Bligaard, T.; Logadottir, A.; Bahn, S.; Hansen, L.; Bollinger, M.; Bengaard, H.; Hammer, B.; Sljivancanin, Z.; Mavrikakis, M.; Xu, Y.; Dahl, S.; Jacobsen, C. Universality in heterogeneous catalysis. *J. Catal.* **2002**, *209*, 275 – 278.

(43) Tauster, S. J.; Fung, S. C.; Baker, R. T. K.; Horsley, J. A. Strong interactions in supported-metal catalysts. *Science* **1981**, *211*, 1121–1125.

(44) Muetterties, E. L. Metal clusters in catalysis III. - Clusters as models for chemisorption processes and heterogeneous catalysis. *B. Soc. Chim. Belg.* **1975**, *84*, 959–986.

(45) Bell, A. T. The impact of nanoscience on heterogeneous catalysis. *Science* **2003**, *299*, 1688–1691.

(46) Moffat, J. *Theoretical Aspects of Heterogeneous Catalysis*; Van Nostrand Reinhold Electrical/Computer Science and Engineering Series; Springer Netherlands, 2013.

(47) Joyner, R.; van Santen, R. *Elementary Reaction Steps in Heterogeneous Catalysis*; Nato Science Series C:; Springer Netherlands, 2012.

(48) Salem, L. The mechanism of the chemical reaction, with recent developments pertaining to heterogeneous catalysis. *Int. J. Quantum Chem.* **1979**, *16*, 321–330.

(49) Jiang, B.; Guo, H. Dynamics in reactions on metal surfaces: A theoretical perspective. *J. Chem. Phys.* **2019**, *150*, 180901.

(50) Petek, H.; Nagano, H.; Weida, M. J.; Ogawa, S. Quantum control of nuclear motion at a metal surface. *J. Phys. Chem. A* **2000**, *104*, 10234–10239.

(51) Petek, H.; Ogawa, S. Surface femtochemistry: Observation and quantum control of frustrated desorption of alkali atoms from noble metals. *Annu. Rev. Phys. Chem.* **2002**, *53*, 507–531.

(52) Szakacs, T.; Lucza, T.; Lorincz, A. Optimal control of quantum systems on metallic surfaces. *Surface Science* **1993**, *296*, 251 – 260.

(53) Nuernberger, P.; Wolpert, D.; Weiss, H.; Gerber, G. Femtosecond quantum control of molecular bond formation. *Proceedings of the National Academy of Sciences* **2010**, *107*, 10366–10370.

(54) Reuß, C.; Shumay, I. L.; Thomann, U.; Kutschera, M.; Weinelt, M.; Fauster, T.; Höfer, U. Control of the dephasing of image-potential states by CO adsorption on Cu(100). *Phys. Rev. Lett.* **1999**, *82*, 153–156.

(55) Güdde, J.; Rohleder, M.; Meier, T.; Koch, S. W.; Höfer, U. Time-resolved investigation of coherently controlled electric currents at a metal surface. *Science* **2007**, *318*, 1287–1291.

(56) Nuernberger, P.; Wolpert, D.; Weiss, H.; Gerber, G. Femtosecond laser-assisted catalytic surface reactions of syngas and their optimization by tailored laser pulses. Ultrafast Phenomena XV. Berlin, Heidelberg, 2007; pp 237–239.

(57) Cui, X.; Wang, C.; Argondizzo, A.; Garrett-Roe, S.; Gumhalter, B.; Petek, H. Transient excitons at metal surfaces. *Nature Physics* **2014**, *10*, 505.

(58) Beye, M. et al. Selective ultrafast probing of transient hot chemisorbed and precursor states of CO on Ru(0001). *Phys. Rev. Lett.* **2013**, *110*, 186101.

(59) Dell'Angela, M. et al. Real-time observation of surface bond breaking with an X-ray laser. *Science* **2013**, *339*, 1302–1305.

(60) Hla, S.-W.; Meyer, G.; Rieder, K.-H. Inducing single-molecule chemical reactions with a UHV-STM: A new dimension for nano-science and technology. *ChemPhysChem* **2001**, *2*, 361–366.

(61) Henzl, J.; Mehlhorn, M.; Gawronski, H.; Rieder, K.-H.; Morgenstern, K. Reversible cis-trans Isomerization of a Single Azobenzene Molecule. *Angewandte Chemie International Edition* **2006**, *45*, 603–606.

(62) Safiei, A.; Henzl, J.; Morgenstern, K. Isomerization of an azobenzene derivative on a thin insulating layer by inelastically tunneling electrons. *Phys. Rev. Lett.* **2010**, *104*, 216102.

(63) Martel, R.; Avouris, P.; Lyo, I.-W. Molecularly adsorbed oxygen species on Si(111)-(7x7): STM-induced dissociative attachment studies. *Science* **1996**, *272*, 385–388.

(64) Avouris, P.; Walkup, R.; Rossi, A.; Akpati, H.; Nordlander, P.; Shen, T.-C.; Abeln, G.; Lyding, J. Breaking individual chemical bonds via STM-induced excitations. *Surface Science* **1996**, *363*, 368 – 377, Dynamical Quantum Processes on Solid Surfaces.

(65) Auburger, P.; Kemeny, I.; Bertram, C.; Ligges, M.; Bockstedte, M.; Bovensiepen, U.; Morgenstern, K. Microscopic insight into electron-induced dissociation of aromatic molecules on ice. *Phys. Rev. Lett.* **2018**, *121*, 206001.

(66) Lauhon, L. J.; Ho, W. Single-molecule chemistry and vibrational spectroscopy: pyridine and benzene on Cu(001). *J. Phys. Chem. A* **2000**, *104*, 2463–2467.

(67) Rusimova, K. R.; Purkiss, R. M.; Howes, R.; Lee, F.; Crampin, S.; Sloan, P. A. Regulating the femtosecond excited-state lifetime of a single molecule. *Science* **2018**, *361*, 1012–1016.

(68) Doppagne, B.; Chong, M. C.; Bulou, H.; Boeglin, A.; Scheurer, F.; Schull, G. Electrofluorochromism at the single-molecule level. *Science* **2018**, *361*, 251–255.

(69) Zhang, L.; Yu, Y.-J.; Chen, L.-G.; Luo, Y.; Yang, B.; Kong, F.-F.; Chen, G.; Zhang, Y.; Zhang, Q.; Luo, Y.; Yang, J.-L.; Dong, Z.-C.; Hou, J. G. Electrically driven single-

photon emission from an isolated single molecule. *Nature Communications* **2017**, *8*, 580.

(70) Li, S.; Czap, G.; Wang, H.; Wang, L.; Chen, S.; Yu, A.; Wu, R.; Ho, W. Bond-selected photodissociation of single molecules adsorbed on metal surfaces. *Phys. Rev. Lett.* **2019**, *122*, 077401.

(71) Morin, M.; Levinos, N. J.; Harris, A. L. Vibrational energy transfer of CO/Cu(100): Nonadiabatic vibration/electron coupling. *J. Chem. Phys.* **1992**, *96*, 3950–3956.

(72) Beckerle, J. D.; Casassa, M. P.; Cavanagh, R. R.; Heilweil, E. J.; Stephenson, J. C. Ultrafast infrared response of adsorbates on metal surfaces: Vibrational lifetime of CO/Pt(111). *Phys. Rev. Lett.* **1990**, *64*, 2090–2093.

(73) Beckerle, J. D.; Cavanagh, R. R.; Casassa, M. P.; Heilweil, E. J.; Stephenson, J. C. Subpicosecond transient infrared spectroscopy of adsorbates. Vibrational dynamics of CO/Pt(111). *J. Chem. Phys.* **1991**, *95*, 5403–5418.

(74) Shirhatti, P. R.; Rahinov, I.; Golibrzuch, K.; Werdecker, J.; Geweke, J.; Altschäffel, J.; Kumar, S.; Auerbach, D. J.; Bartels, C.; Wodtke, A. M. Observation of the adsorption and desorption of vibrationally excited molecules on a metal surface. *Nat. Chem.* **2018**, *10*, 592–598.

(75) Ueba, H. Vibrational state of the chemisorbed molecule on metal surfaces: Role of electron-hole pair excitation. *J. Chem. Phys.* **1982**, *77*, 3759–3766.

(76) Schönhammer, K.; Gunnarsson, O. Energy dissipation at metal surfaces: Electronic versus vibrational excitations. *J. Electron Spectrosc.* **1983**, *29*, 91 – 103.

(77) Ran, Q.; Matsiev, D.; Auerbach, D. J.; Wodtke, A. M. Observation of a change of vibrational excitation mechanism with surface temperature: HCl collisions with Au(111). *Phys. Rev. Lett.* **2007**, *98*, 237601.

(78) Grotemeyer, M.; Pehlke, E. Electronic energy dissipation during scattering of vibrationally excited molecules at metal surfaces: Ab initio simulations for HCl/Al(111). *Phys. Rev. Lett.* **2014**, *112*, 043201.

(79) Rittmeyer, S. P.; Bukas, V. J.; Reuter, K. Energy dissipation at metal surfaces. *Advances in Physics: X* **2018**, *3*, 1381574.

(80) Novko, D.; Tremblay, J. C.; Alducin, M.; Juaristi, J. I. Ultrafast transient dynamics of adsorbates on surfaces deciphered: The case of CO on Cu(100). *Phys. Rev. Lett.* **2019**, *122*, 016806.

(81) Ge, A.; Rudshteyn, B.; Zhu, J.; Maurer, R. J.; Batista, V. S.; Lian, T. Electron-hole-pair-induced vibrational energy relaxation of rhenium catalysts on gold surfaces. *J. Phys. Chem. Lett.* **2018**, *9*, 406–412.

(82) Mercurio, G.; McNellis, E. R.; Martin, I.; Hagen, S.; Leyssner, F.; Soubatch, S.; Meyer, J.; Wolf, M.; Tegeder, P.; Tautz, F. S.; Reuter, K. Structure and Energetics of Azobenzene on Ag(111): Benchmarking Semiempirical Dispersion Correction Approaches. *Phys. Rev. Lett.* **2010**, *104*, 036102.

(83) Sony, P.; Puschnig, P.; Nabok, D.; Ambrosch-Draxl, C. Importance of van der Waals interaction for organic molecule-metal junctions: Adsorption of thiophene on Cu(110) as a prototype. *Phys. Rev. Lett.* **2007**, *99*, 176401.

(84) Mura, M.; Gulans, A.; Thonhauser, T.; Kantorovich, L. Role of van der Waals interaction in forming molecule-metal junctions: flat organic molecules on the Au(111) surface. *Phys. Chem. Chem. Phys.* **2010**, *12*, 4759–4767.

(85) Li, G.; Tamblyn, I.; Cooper, V. R.; Gao, H.-J.; Neaton, J. B. Molecular adsorption on metal surfaces with van der Waals density functionals. *Phys. Rev. B* **2012**, *85*, 121409.

(86) Bilic, A.; Reimers, J. R.; Hush, N. S. Adsorption of pyridine on the gold(111) Surface: Implications for alligator clips for molecular wires. *J. Phys. Chem. B* **2002**, *106*, 6740–6747.

(87) Ruiz, V. G.; Liu, W.; Zojer, E.; Scheffler, M.; Tkatchenko, A. Density-functional theory with screened van der Waals interactions for the modeling of hybrid inorganic-organic systems. *Phys. Rev. Lett.* **2012**, *108*, 146103.

(88) Díaz-Tendero, S.; Alcamí, M.; Martín, F. Density functional theory study of the structure and vibrational modes of acrylonitrile adsorbed on Cu(100). *Phys. Chem. Chem. Phys.* **2013**, *15*, 1288–1295.

(89) Robledo, M.; Díaz-Tendero, S. Exploring the adsorption and the potential energy surface of acrylonitrile on Cu(100) and Cu(100) coated with NaCl layers. *J. Phys. Chem. C* **2015**, *119*, 15125–15136.

(90) Robledo, M.; Pacchioni, G.; Martín, F.; Alcamí, M.; Díaz-Tendero, S. Adsorption of benzene on Cu(100) and on Cu(100) covered with an ultrathin NaCl film: molecule-substrate interaction and decoupling. *J. Phys. Chem. C* **2015**, *119*, 4062–4071.

(91) Chiter, F.; Nguyen, V. B.; Tarrat, N.; Benoit, M.; Tang, H.; Lacaze-Dufaure, C. Effect of van der Waals corrections on DFT-computed metallic surface properties. *Mater. Res. Express* **2016**, *3*, 046501.

(92) Andersson, Y.; Hult, E.; Rydberg, H.; Apell, P.; Lundqvist, B. I.; Langreth, D. C. In *Electronic density functional theory: recent progress and new directions*; Dobson, J. F., Vignale, G., Das, M. P., Eds.; Springer US: Boston, MA, 1998; pp 243–260.

(93) Ruiz, V. G.; Liu, W.; Tkatchenko, A. Density-functional theory with screened van der Waals interactions applied to atomic and molecular adsorbates on close-packed and non-close-packed surfaces. *Phys. Rev. B* **2016**, *93*, 035118.

(94) Berland, K.; Cooper, V. R.; Lee, K.; Schröder, E.; Thonhauser, T.; Hyldgaard, P.; Lundqvist, B. I. Van der Waals forces in density functional theory: a review of the vdW-DF method. *Rep. Prog. Phys.* **2015**, *78*, 066501.

(95) Dion, M.; Rydberg, H.; Schröder, E.; Langreth, D. C.; Lundqvist, B. I. Van der Waals density functional for general geometries. *Phys. Rev. Lett.* **2004**, *92*, 246401.

(96) Román-Pérez, G.; Soler, J. M. Efficient implementation of a van der Waals density functional: Application to Double-wall carbon nanotubes. *Phys. Rev. Lett.* **2009**, *103*, 096102.

(97) Klimeš, J. c. v.; Bowler, D. R.; Michaelides, A. Van der Waals density functionals applied to solids. *Phys. Rev. B* **2011**, *83*, 195131.

(98) Kresse, G.; Furthmühller, J. Efficiency of ab-initio total energy calculations for metals and semiconductors using a plane-wave basis set. *Comput. Mat. Sci.* **1996**, *6*, 15–50.

(99) Kresse, G.; Furthmühller, J. Efficient iterative schemes for ab initio total-energy calculations using a plane-wave basis set. *Phys. Rev. B* **1996**, *54*, 11169.

(100) Klimeš, J. c. v.; Bowler, D. R.; Michaelides, A. Chemical accuracy for the van der Waals density functional. *J. Phys.-Condens. Mat.* **2010**, *22*, 022201.

(101) Björk, J.; Stafström, S. Adsorption of large hydrocarbons on coinage metals: a van der Waals density functional study. *ChemPhysChem* **2014**, *15*, 2851–2858.

(102) Gautier, S.; Steinmann, S. N.; Michel, C.; Fleurat-Lessard, P.; Sautet, P. Molecular adsorption at Pt(111). How accurate are DFT functionals? *Phys. Chem. Chem. Phys.* **2015**, *17*, 28921–28930.

(103) Blöchl, P. E. Projector augmented-wave method. *Phys. Rev. B* **1994**, *50*, 17953–17979.

(104) Kresse, G.; Joubert, D. From ultrasoft pseudopotentials to the projector augmented-wave method. *Phys. Rev. B* **1999**, *59*, 1758–1775.

(105) Monkhorst, H. J.; Pack, J. D. Special points for Brillouin-zone integrations. *Phys. Rev. B* **1976**, *13*, 5188–5192.

(106) Methfessel, M.; Paxton, A. T. High-precision sampling for Brillouin-zone integration in metals. *Phys. Rev. B* **1989**, *40*, 3616–3621.

(107) Bader, R. F. W. A quantum theory of molecular structure and its applications. *Chem. Rev.* **1991**, *91*, 893–928.

(108) Bader, R. F. W. *Atoms in Molecules: A Quantum Theory*; Oxford University Press, USA, 1994.

(109) Tang, W.; Sanville, E.; Henkelman, G. A grid-based Bader analysis algorithm without lattice bias. *J. Phys. Condens. Mat.* **2009**, *21*, 084204.

(110) Sanville, E.; Kenny, S. D.; Smith, R.; Henkelman, G. Improved grid-based algorithm for Bader charge allocation. *J. Comput. Chem.* **2007**, *28*, 899–908.

(111) Henkelman, G.; Arnaldsson, A.; Jonsson, H. A fast and robust algorithm for Bader decomposition of charge density. *Comp. Mat. Sci.* **2006**, *36*, 354 – 360.

(112) Frisch, M. J. et al. Gaussian 09 Revision E.01, Gaussian Inc. Wallingford CT 2013. 2013.

(113) Blanksby, S. J.; Ellison, G. B. Bond dissociation energies of organic molecules. *Accounts of Chemical Research* **2003**, *36*, 255–263.

(114) Reguera, E. Materials for hydrogen storage in nanocavities: Design criteria. *Int. J. Hydrogen Energ.* **2009**, *34*, 9163 – 9167.

(115) Toader, M.; Shukrynau, P.; Knupfer, M.; Zahn, D. R. T.; Hietschold, M. Site-dependent donation/backdonation charge transfer at the CoPc/Ag(111) interface. *Langmuir* **2012**, *28*, 13325–13330.

(116) Gladh, J.; Öberg, H.; Li, J.; Ljungberg, M. P.; Matsuda, A.; Ogasawara, H.; Nilsson, A.; Pettersson, L. G. M.; Öström, H. X-ray emission spectroscopy and density functional study of CO/Fe(100). *J. Chem. Phys.* **2012**, *136*, 034702.

(117) Verma, C. B.; Quraishi, M.; Singh, A. 2-Aminobenzene-1,3-dicarbonitriles as green corrosion inhibitor for mild steel in 1 M HCl: Electrochemical, thermodynamic, surface and quantum chemical investigation. *J. Taiwan Inst. Chem. E.* **2015**, *49*, 229 – 239.

(118) Simpson, S.; Hooper, J.; Miller, D. P.; Kunkel, D. A.; Enders, A.; Zurek, E. Modulating bond lengths via backdonation: A first-principles investigation of a quinonoid zwitterion adsorbed to coinage metal surfaces. *J. Phys. Chem. C* **2016**, *120*, 6633–6641.

(119) Vázquez, H.; Dappe, Y. J.; Ortega, J.; Flores, F. Energy level alignment at metal/organic semiconductor interfaces: "Pillow" effect, induced density of interface states, and charge neutrality level. *J. Chem. Phys.* **2007**, *126*, 144703.

(120) Hamada, Y.; Nishimura, Y.; Tsuboi, M. Infrared spectrum of trans-acrolein. *Chem. Phys.* **1985**, *100*, 365 – 375.

(121) Tornero, J.; Telle, H.; García, G.; González-Ureña, A. Vibrational excitation of adsorbed molecules by photoelectrons of very low energy: acrylonitrile on Cu(100). *Phys. Chem. Chem. Phys.* **2011**, *13*, 8475–8484.

Graphical TOC Entry